ARTICLE

Kinetic evidence in favor of glyoxalase III and against deglycase activity of DJ-1

Joonhyeok Choi[1] [iD] | Sungho Tak[1] | Hoe-Myung Jung[1,2] | Soyoung Cha[1] | Eunha Hwang[1] | Donghan Lee[1] | Joon-Hwa Lee[3] | Kyoung-Seok Ryu[1,2] [iD] | Chankyu Park[4]

[1]Ochang Center, Korea Basic Science Institute, Cheongju-Si, South Korea

[2]Department of Bio-Analytical Science, University of Science and Technology, Daejeon, South Korea

[3]Department of Chemistry and RINS, Gyeongsang National University, Gyeongnam, South Korea

[4]Department of Biological Sciences, KAIST, Daejeon, South Korea

Correspondence
Joon-Hwa Lee, Department of Chemistry and RINS, Gyeongsang National University, Gyeongnam, 52828 South Korea.
Email: joonhwa@gnu.ac.kr

Kyoung-Seok Ryu, Ochang center, Korea Basic Science Institute, 162 Yeongudanji-Ro, Ochang-Eup, Cheongju-Si, Chungcheongbuk-Do 28119, South Korea.
Email: ksryu@kbsi.re.kr

Funding information
KBSI, Grant/Award Numbers: C140130, C130000; National Research Foundation of Korea, Grant/Award Numbers: 2023R1A2C1006973, 2022H1D3A2A02093655, 2020R1A2C1006909, 2022R1A4A1021817; Samsung Science & Technology Foundation, Grant/Award Number: SSTF-BA1701-10

Review Editor: Aitziber L. Cortajarena

Abstract

DJ-1, a protein encoded by *PARK7* plays a protective role against neurodegeneration. Since its glyoxalase III activity catalyzing methylglyoxal (MG) to lactate was discovered, DJ-1 has been re-established as a deglycase decomposing the MG-intermediates with amino acids and nucleotides (hemithioacetal and hemiaminal) rather than MG itself, but it is still debatable. Here, we have clarified that human DJ-1 directly recognizes MG, and not MG-intermediates, by monitoring the detailed catalytic processes and enantiomeric lactate products. The hemithioacetal intermediate between C106 of ^{15}N-labeled DJ-1 (^{15N}DJ-1) and MG was also monitored by NMR. TRIS molecule formed stable diastereotopic complexes with MG (K_d, 1.57 ± 0.27 mM) by utilizing its three OH groups, which likely disturbed the assay of deglycase activity. The low k_{cat} of DJ-1 for MG and its MG-induced structural perturbation may suggest that DJ-1 has a regulatory function as an in vivo sensor of reactive carbonyl stress.

KEYWORDS
Deglycase, DJ-1, glyoxalase III, ITC, methylglyoxal, NMR, reactive carbonyl species

1 | INTRODUCTION

Since human DJ-1 was first identified as a novel onco-gene transforming NIH3T3 cells via a Ras-dependent signal transduction pathway (Nagakubo et al., 1997), mutations in DJ-1 (DJ-1) are known to cause the early onset of Parkinson disease (PD; Bonifati et al., 2003). DJ-1 protects dopaminergic neurons from cell death in PD, and its various functions, including as molecular chaperone, protease, glyoxalase III, transcriptional regulator, and molecular sensor of oxidative stress, have been reported to date (Ariga et al., 2013; Chen et al., 2010; Dolgacheva et al., 2019; Lee et al., 2003). To explain the multiple roles of DJ-1, it was also reported that DJ-1 specifically binds and suppresses a set of mRNAs with GG/CC-rich sequence including mitochondrial transcripts, components of the PTEN/Akt pathway and genes involved in glutathione (GSH) metabolism (van der Brug et al., 2008). Although these pleiotropic functions of DJ-1 appear to be associated with the oxidized C106 residue (sulfinic acid), the detailed molecular mechanisms remain unknown (Ariga et al., 2013; Dolgacheva et al., 2019). Nevertheless, it is clear that the presence of the DJ-1 gene (PARK7) is important for protecting cells from oxidative stress and maintaining mitochondrial homeostasis in dopaminergic neurons (Canet-Aviles et al., 2004; Guzman et al., 2010).

Oxidative stress is associated with increased sugar metabolism in neuronal cells, which also produces highly toxic by-products of glycolysis, namely reactive carbonyl species (RCSs) of methylglyoxal (MG) and glyoxal (GO). RCSs result in advanced glycation end products (AGEs) of proteins and nucleic acids that are involved in aging-related diseases, including cancer, neurodegenerative diseases, and diabetes (Allaman et al., 2015). MG forms reversible early glycation adducts, and the ultimate stable AGEs result from subsequent and spontaneous chemical rearrangements (Jun & Kool, 2020; Richarme et al., 2015). Therefore, glyoxalase III activity is important for maintaining cellular homeostasis under oxidative stress, that is depletion of GSH, since the more active glyoxalase I/II system utilizes GSH as a cofactor (Allaman et al., 2015). The characterization of the DJ-1 glyoxalase III activity was initiated by an independent study of *Escherichia coli* RbsD protein that was proven to be a novel pyranase of D-ribose, one kind of mutarotase, to accelerate the conversion between β-ribopyranose and β-ribofuranose (Ryu et al., 2004). Shortly thereafter, the accumulation of toxic RCSs of MG and GO caused by overexpression of RbsD, which increases the metabolism of D-ribose, was found to be the cause of *E. coli* death (Kim et al., 2004). Subsequent fractionation and

proteomic studies based on the glyoxalase III activity assay using the extract of *E. coli* K-12 revealed that Hsp31, the *hchA* gene product, is glyoxalase III (Subedi et al., 2011). As Hsp31 is a member of the DJ-1/ThiJ/PfpI superfamily, and the structural studies also showed that DJ-1 and Hsp31 share an evolutionarily conserved domain (Lee et al., 2003), it has also been proven that DJ-1 has glyoxalase III activity (Lee et al., 2012). However, DJ-1 has a wider active-site pocket and less conserved active-site residues as compared to *Arabidopsis thaliana* DJ-1d (atDJ-1d) and Hsp31; thus, its k_{cat} value is lower than those of atDJ-1d and Hsp31 (DJ-1: 0.0272 s^{-1}; atDJ-1d: 0.692 s^{-1}; Hsp31: 1.47 s^{-1} for phenylglyoxal [PG]) (Choi et al., 2014).

On the other hand, it was first reported that DJ-1 is not glyoxalase III, but rather a deglycase to decompose MG intermediate complexes with amino acids such as *N*-acetyl Cys (NAC), *N*-acetyl Lys (NAK), and *N*-acetyl Arg (NAR; Richarme et al., 2015). Later, it was also reported that DJ-1 and its bacterial homologs (Hsp31, YhbO, and YajL) specifically repair the reversible glycated guanosine 5′-triphosphate (GTP aminocarbinol), but not its delayed end-products, namely imidazopurinones and carboxyethyl-deoxyguanosine (Richarme et al., 2017). Nevertheless, there is still a debate regarding the deglycase activity of DJ-1 including potential TRIS buffer artifacts and the D/L-stereochemistry of the lactate products (Pfaff et al., 2017; Richarme, 2017). It was recently reported that the apparent deglycase activity of DJ-1 is the consequence of fast equilibrium between MG and hemithioacetals, likely resulting in the misinterpretation of glyoxalase III as deglycase (Andreeva et al., 2019; Gao et al., 2023; Mazza et al., 2022). However, detailed kinetic data of DJ-1 activities have not yet been reported for GTP aminocarbinol, likely due to difficulty of UV monitoring. The debates on DJ-1 enzyme activity regarding its glyoxalase III versus deglycase activities have also been clearly summarized in a recent review article (Jun & Kool, 2020).

Here, we attempted to resolve two different activities of DJ-1 (glyoxalase III and deglycase) in the same lineage of enzymatic reactions via direct monitoring of the time-dependent enzymatic reactions using isothermal titration calorimetry (ITC) and NMR techniques. DJ-1 does not seem to have deglycase activity, but only displayed glyoxalase III activity both for hemithioacetal and hemiaminal. It was also confirmed that TRIS molecule formed stable diastereotopic covalent complexes with MG. Structural perturbation of the MG-hemithioacetal of the DJ-1 C106 residue (MG-C106) was also analyzed using ^{1}H-^{15}N heteronuclear single quantum coherence (HSQC) spectra.

2 | RESULTS

2.1 | Determination of the preliminary parameters for detailed enzyme kinetics experiments

First, the C106 active site residue of DJ-1 is highly susceptible to oxidation because of its low pK_a value (5.4 ± 0.1; Witt et al., 2008), and the identical secondary structure of the C106-sulfinic acid (—SO$_2$) form with that of the native one was also characterized by triple resonance NMR experiments (Barbieri & Luchinat, 2019). We recently established a column chromatography method to separate native DJ-1 from oxidized one (Choi et al., 2022). The exact concentration of the MG stock solution was back-calculated from the MG-titration curves with the fixed concentration of NAC (100 mM) using UV absorption at 288 nm (Figure S1). The determined extinction coefficient (250 ± 11 M^{-1}·cm^{-1}) of the MG-hemiacetal of NAC (MG-NAC) was much higher than the previously reported value (98 ± 5 M^{-1}·cm^{-1}; Lo et al., 1994), but was similar to the recently reported values of MG-NAC (300 M^{-1}·cm^{-1}; Andreeva et al., 2019).

The equilibrium constants (K_d, =1/K_{eq}) of the MG intermediates (hemithioacetal and hemiaminal) were first determined before detailed kinetic studies (Table 1). The K_d values of the MG-hemiacetal of GSH (MG-GSH) and MG-NAC were measured using both one-dimensional (1D) ^{1}H-NMR and UV absorption, but that of the MG hemiaminal of guanosine 5′-monophosphate (MG-GMP) was determined only by 1D ^{1}H-NMR (Table 1 and Figure S2). The K_d values of MG-GSH (NMR, 1.67 mM; UV, 1.92 mM) and MG-NAC (NMR, 1.70 mM; UV, 1.89 mM) were similar to the previously reported value of MG-GSH (1.96 mM; Andreeva et al., 2019). The K_d value of MG-GMP was determined from the equilibrium NMR spectra (0.98 mM). The equilibrium constants of the MG-hemiaminals of NAR (MG-NAR) and NAK (MG-NAK) could not be determined because the reaction between 10 mM MG and 3 mM NAR was slow (half time to reach equilibrium ~9 h), and the reaction between MG and NAK was too slow to detect the 1D peaks of the MG-NAK intermediate even after overnight incubation (Figure S3). Therefore, MG-NAR and MG-NAK could not be tested for detailed kinetic studies.

2.2 | ITC monitoring of the MG catalysis by DJ-1 protein

Indirect detection of MG via a chemical reaction using 2,3-dinitrophenylhydrazine (Andreeva et al., 2019; Lee et al., 2012) may cause difficulties in enzyme kinetics

**TABLE 1** Equilibrium and kinetic parameters of the DJ-1-mediated MG catalysis.

K_d (mM)	By NMR	By UV
MG-GSH	1.67 ± 0.14	1.92 ± 0.06
MG-NAC	1.70 ± 0.26	1.89 ± 0.14
MG-GMP	0.98 ± 0.27	
MG-TRIS	1.57 ± 0.27	
k_{off} (s^{-1}, =k_{-4})	MG-NAC	MG-GMP
25°C	0.153 ± 0.030	0.00078 ± 0.00022
35°C	0.313 ± 0.042	0.00359 ± 0.00017
By ITC[a]	K_m (mM)	k_{cat} (s^{-1})
20°C	0.157 ± 0.030	0.0758 ± 0.0046
25°C	0.284 ± 0.051	0.117 ± 0.001
30°C	0.388 ± 0.055	0.180 ± 0.004
35°C	0.463 ± 0.080	0.261 ± 0.002
Equilibrium between MG′ and MG″ at 25°C		
k_3 (s^{-1})[b]	0.0107 ± 0.0002	
k_{-3} (s^{-1})	0.00667 ± 0.0001	
Time-course 1D NMR for MG alone at 25°C		
K_m (mM)	0.387 ± 0.007	
k_{cat} (s^{-1})	0.108 ± 0.001	
k_3 (s^{-1})	0.01032 ± 0.00002	
k_{-3} (s^{-1})	0.00667[c]	
Time-course 1D NMR for MG-NAC at 25°C		
K_m (mM)	0.432 ± 0.043	
k_{cat} (s^{-1})	0.109 ± 0.004	
k_3 (s^{-1})	0.0100 ± 0.0004	
k_{-3} (s^{-1})	0.00667[c]	
k_4^{app} (mM^{-1}·s^{-1})	0.052 ± 0.001	
k_{-4} (s^{-1})	0.133[c]	
Time-course 1D NMR for MG-GMP at 25°C		
K_m (mM)	0.475 ± 0.014	
k_{cat} (s^{-1})	0.101 ± 0.002	
k_3 (s^{-1})	0.0111 ± 0.0003	
k_{-3} (s^{-1})	0.00667[c]	
k_4^{app} (mM^{-1}·s^{-1})	0.00126 ± 0.00001	
k_{-4} (s^{-1})	0.000840[c]	

Abbreviations: ITC, isothermal titration calorimetry; MG, methylglyoxal; MG-GMP, MG hemiaminal of guanosine 5′-monophosphate; MG-NAC, MG-hemiacetal of N-acetyl Cys.

[a]Error value was obtained from two different analyses using the Michaelis–Menten equation and the direct fitting of the whole ITC profile, otherwise means a fitting error.

[b]The k_3 was calculated from the measured k_{-3} using the ratio of MG′ and MG″.

[c]The k_{-3} and k_{-4} values were fixed to the experimental values during the fitting with Equations (3–6), in which the k_{-4} values at 25°C were back-calculated from the Arrhenius plots (Figure S4C).
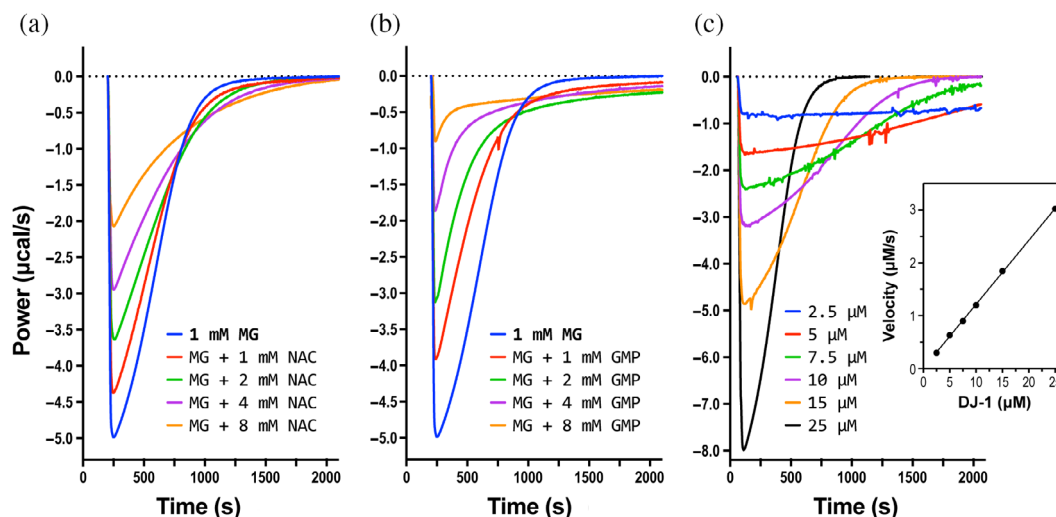
FIGURE 1 Isothermal titration calorimetry (ITC)-monitoring the DJ-1-mediated methylglyoxal (MG) catalysis. The single-shot ITC measurements using 15 μM DJ-1 protein were executed as increasing the concentrations of (a) *N*-acetyl Cys and (b) GMP, respectively. (c) The ITC profiles of the MG catalysis were measured by varying the concentrations of DJ-1. The V_{max} values were linearly increased as increasing the concentrations of DJ-1 (inset).

studies, which may also result in an unpredicted artifact. Therefore, the presence of a direct method to measure the MG catalysis would be necessary. UV absorption can be used to monitor MG-NAC hemithioacetal, but is not suitable for detecting MG-GMP hemiaminal. In our studies, ITC and 1D ^{1}H-NMR methods were used to resolve the debating enzyme activities. A single injection ITC method was first used to monitor DJ-1-mediated MG catalysis, in which the conversion of MG to lactate was an exothermic reaction (Figure 1). It was previously reported that DJ-1 forms filamentous aggregates in phosphate buffer (Cha et al., 2008). However, any decreasing activity of DJ-1 was not detected in phosphate buffer as compared to HEPES buffer at pH 7.0 (not shown), which was likely due to different experimental conditions such as a low concentration of DJ-1.

The K_m and k_{cat} values of DJ-1 at 35 °C were determined to be 0.520 mM and 0.263 s^{-1}, respectively (Table 1). To determine the deglycase activity of DJ-1 via ITC experiments, MG was preincubated with NAC or GMP, and then the same amount of DJ-1 protein was injected. As the concentration of NAC increased, the exothermic ITC curves were reduced and delayed (Figure 1a). This phenomenon became more apparent with increasing GMP concentration (Figure 1b). The decreasing exotherm was due to heat compensation by the endothermic reaction resulting from the dissociation of MG-NAC hemithioacetal (not shown) and MG-GMP hemiaminal (Figure S4b). However, the delayed reactions were hardly explained by the deglycase activity of DJ-1, which was assumed to preferentially decompose MG intermediates rather than MG. We measured the

spontaneous dissociation rates (k_{off}) of MG-NAC and MG-GMP, which were monitored by UV spectroscopy at 288 nm and ITC, respectively (Figure S4a,b).

The rapid dissociation process of MG-NAC could not be analyzed by ITC due to the limited time resolution of the measurement. The k_{-4} value of MG-GMP (0.00359 s^{-1}) was much slower than that of MG-NAC (0.313 s^{-1}) at 35°C (Table 1). A more delayed reaction in the presence of GMP, as compared to in the case of NAC, could be possible when DJ-1 preferentially recognizes MG as its substrate.

It was previously reported that deglycase activity increases depending on the square of DJ-1 concentration due to the intermolecular recognition of MG-modified DJ-1 by different DJ-1 proteins (Richarme et al., 2015). Therefore, the enzymatic reactions of MG were monitored using ITC at different concentrations of DJ-1. Since the reactivity of Arg and Lys residues to MG was very low (Figure S3), 7 Arg and 16 Lys residues of DJ-1 hardly influence the relatively short ITC measurements. Although two Cys residues (C46 and C53) besides the catalytic C106 might have contributed to the deglycase activity, the velocity of the MG catalysis linearly increased with increasing concentrations of DJ-1 (Figure 1C).

2.3 | NMR monitoring of DJ-1-mediated MG catalysis

We performed NMR kinetic experiments to resolve the detailed mechanism of DJ-1-mediated MG catalysis at 25°C. To monitor the changes in all reaction components
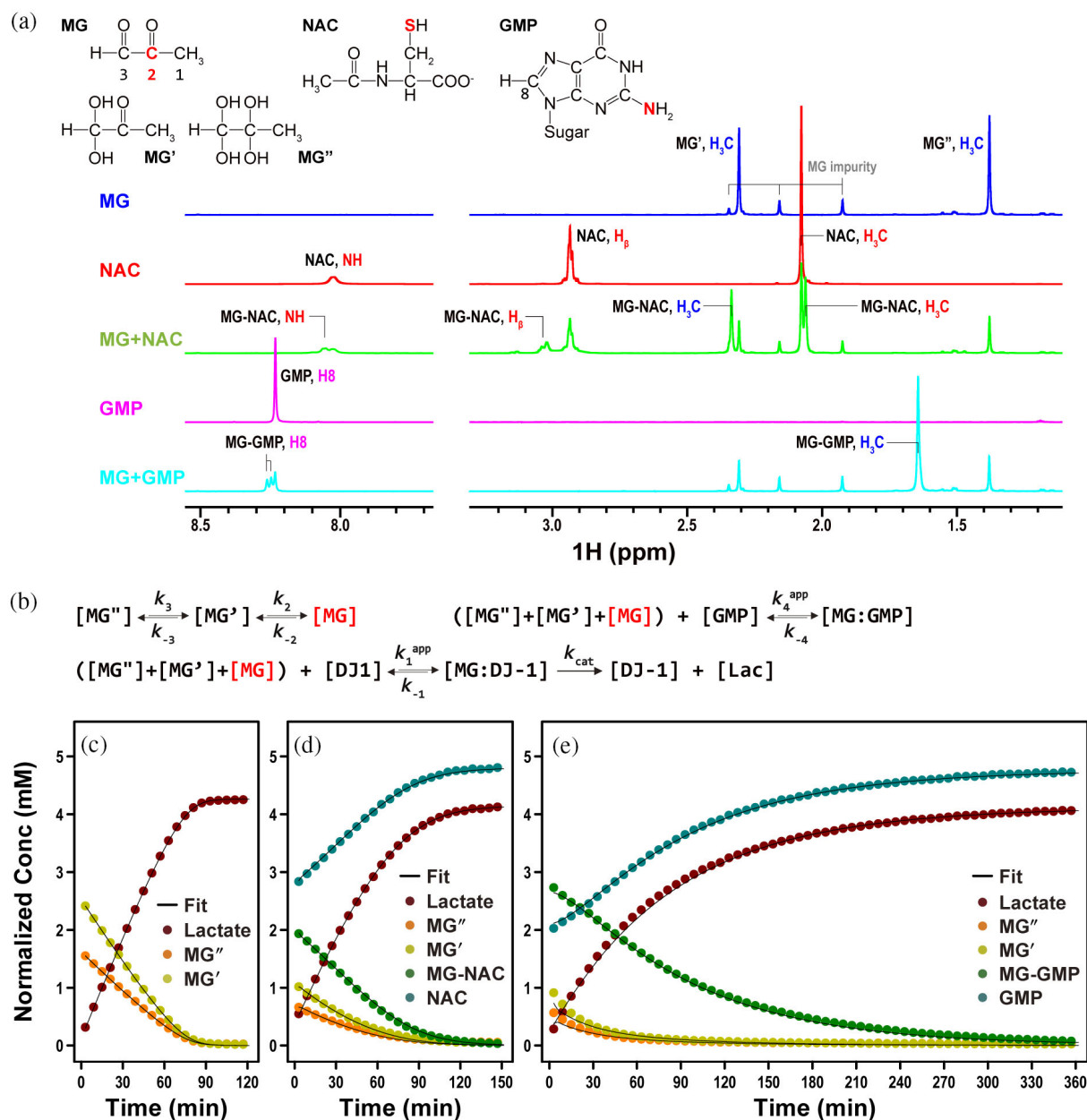
FIGURE 2 Time-coursed monitoring of the DJ-1-mediated methylglyoxal (MG) catalysis in the absence and presence of *N*-acetyl Cys (NAC) and guanosine 5′-monophosphate (GMP). (a) The 1D NMR spectra of MG alone, MG-hemiacetal of NAC (MG-NAC), and MG hemiaminal of GMP (MG-GMP) were recorded using 700 MHz NMR spectrometer at 25°C. Two methyl peaks of MG are corresponded to the monohydrated and dihydrated forms (MG′ and MG″), respectively; however, that of the nonhydrated form was not identified. The nitrogen and sulfur atoms of GMP and NAC (red) form the covalent bond with the C2 atom of MG (red), resulting in MG-GMP and MG-NAC, respectively. There is only one methyl peak corresponding to MG-NAC (or MG-GMP), which indicates no additional hydration to the MG-intermediates. (b) The DJ-1-mediated MG-catalysis in the presence of GMP consists of (i) the equilibrium of MG species and GMP, and (ii) the MG catalysis by DJ-1. In the case of MG-NAC, the term GMP is changed to NAC. Since the nonhydrated form of MG is not visible due to a tiny amount in solution, the sum of [MG′] and [MG″] was used as the free MG concentration. The concentrations of the reaction components were estimated by integrating each peak of the time-course 1D NMR spectra; (c) MG alone, (d) MG-NAC, and (e) MG-GMP.

in real time, the time-course 1D NMR spectra were acquired for three different DJ-1 reactions: (i) MG alone, (ii) MG-NAC, and (iii) MG-GMP. MG mostly exists as MG′ (monohydrated) and MG″ (dihydrated) in solution, and its nonhydrated form was not identified in the 1D

NMR spectra (Figure 2a). To describe the detailed kinetics NMR data based on glyoxalase III activity, DJ-1-mediated MG catalysis was divided into three processes (Figure 2b): (i) equilibrium among different MG species, (ii) lactate (LAC) produced via DJ-1 enzyme activity

(v_{DJ1}), and (iii) equilibrium between MG and GMP (or NAC). The overall reaction patterns clearly show that the delayed lactate production was likely due to the slow dissociation of MG (DJ-1 substrate) from MG-NAC and MG-GMP (Figures 2c–e, and S5). Since (i) the equilibrium among MG′, MG″, and MG was much faster than the V_{max} value of DJ-1-mediated MG catalysis, and (ii) the dissociation rate (k_{-4}) of MG-GMP (0.00078 s^{-1}) was much slower than that of MG-NAC (0.153 s^{-1}) at 25°C (Table 1), the methyl peaks of both MG′ and MG″ were preferentially and simultaneously decreased, and the decreasing methyl peaks of MG-GMP were apparently retarded (Figure 2e).

Equations (3–6) in Section 5 summarize the time-dependent concentration changes for each reaction component. The time-course enzyme kinetic data of MG alone, MG-NAC and MG-GMP were fitted to Equations (3–6) (Figure 2c–e). Although the k_3 and k_{-3} values at 37°C (0.051 and 0.021 s^{-1}, respectively) were previously reported (Rae et al., 1990), k_3 and k_{-3} values (0.0107 and 0.00667 s^{-1}, respectively) were measured again at 25°C using the saturation-transfer ^{1}H-NMR technique (Table 1) (Robinson et al., 1984). Equation (5) and the terms of [GMP] and [MG:GMP] in Equations (3) and (4) were not used for the fitting of the kinetic data of MG alone. The values of k_{-3} and k_{-4} (k_{off} in Figure S4) were fixed to the measured values during the fitting processes. Although the K_m little increased in the cases of MG-NAC and MG-GMP compared to the case of MG alone, the fit parameters of all cases were reasonably in agreement with the expected values (Table 1). Overall, all time-course data were well reproduced by fitting with the differential equations derived from the assumption of glyoxalase III activity (Figure 2c–e).

2.4 | DJ-1-mediated MG catalysis only produces L-lactate

The differential production of D/L-lactates from MG seems to be a critical indicator for discrimination between glyoxalase III and deglycase activities (Jun & Kool, 2020). First, the detailed molecular mechanism by which DJ-1 produces only L-lactate was previously determined via x-ray crystallographic and molecular simulation studies (Choi et al., 2014). However, it has also been reported that DJ-1 produces D/L-lactate mixture (33/67%) from MG-NAC and 100% L-lactate from MG-NAR (Richarme et al., 2015). For an accurate measurement of the enantiomeric D/L-lactate products, we first estimated the real activities of D-lactate dehydrogenase (LDH) and L-LDH for the same concentration (0.2 mM) of D-lactate and L-lactate, respectively. Interestingly,
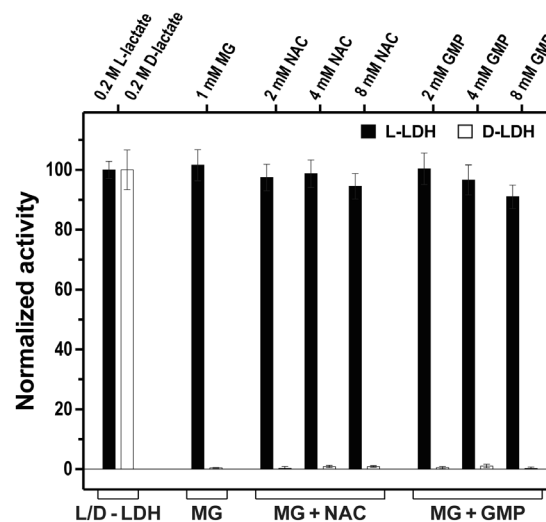

FIGURE 3 Analysis of the D/L-lactate products from the DJ-1-mediated methylglyoxal (MG) catalysis. The lactate products were generated from the complete reactions of 1 mM MG alone, MG-hemiacetal of N-acetyl Cys, and MG hemiaminal of guanosine 5′-monophosphate in the presence of 20 μM DJ-1. The products were 5 times diluted for the enzymatic assay of D-lactate dehydrogenase (LDH) and L-LDH. First, the relative activities of D-LDH and L-LDH at pH 9.5 were adjusted to be the same using 0.2 mM D-lactate and L-lactate, respectively, and then the same activity of D-LDH and L-LDH were used for the assessment of the enantiomeric lactate products. The production of D-lactate was not detected in all the cases.

12 times higher amount of D-LDH was required for the same activity of L-LDH at pH 9.5. Although the production of D/L-lactates was evaluated for different substrates (MG, MG-NAC, and MG-GMP), D-lactate was not detected in any of the cases (Figure 3).

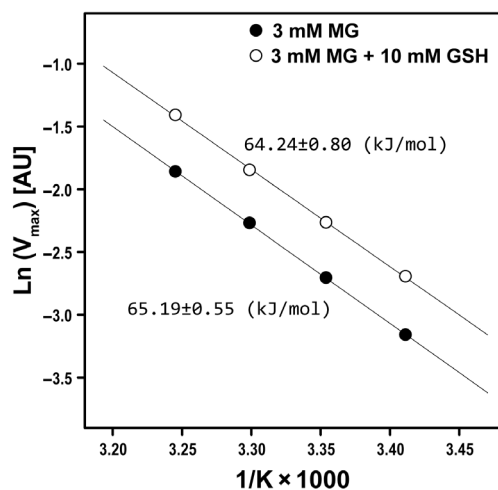## 2.5 | The intermediate state of DJ-1-mediated MG catalysis shows that DJ-1 is not a deglycase

The simulation of the CSs using the NMR Predict program (Castillo et al., 2011) for different chemical structures of MG-NAC molecules showed that MG-NAC likely exists in a nonhydrated form, and thus the C2 of MG-NAC could be accessible to the sulfur atom of C106 (Figure 4a). If DJ-1 preferentially recognizes the MG-NAC, the sulfur atom of C106 is only accessible to C2 of MG-NAC, and thus the HSQC spectra of the ^{15}N-labeled DJ-1 (^{15N}DJ-1) complexed with MG and MG-NAC were likely to be different. The very low k_{cat} value of the catalysis (0.117 s^{-1} at 25°C) made it possible to record the HSQC spectra of the MG attached ^{15N}DJ-1 protein. The time-coursed HSQC spectra of ^{15N}DJ-1 were recorded in
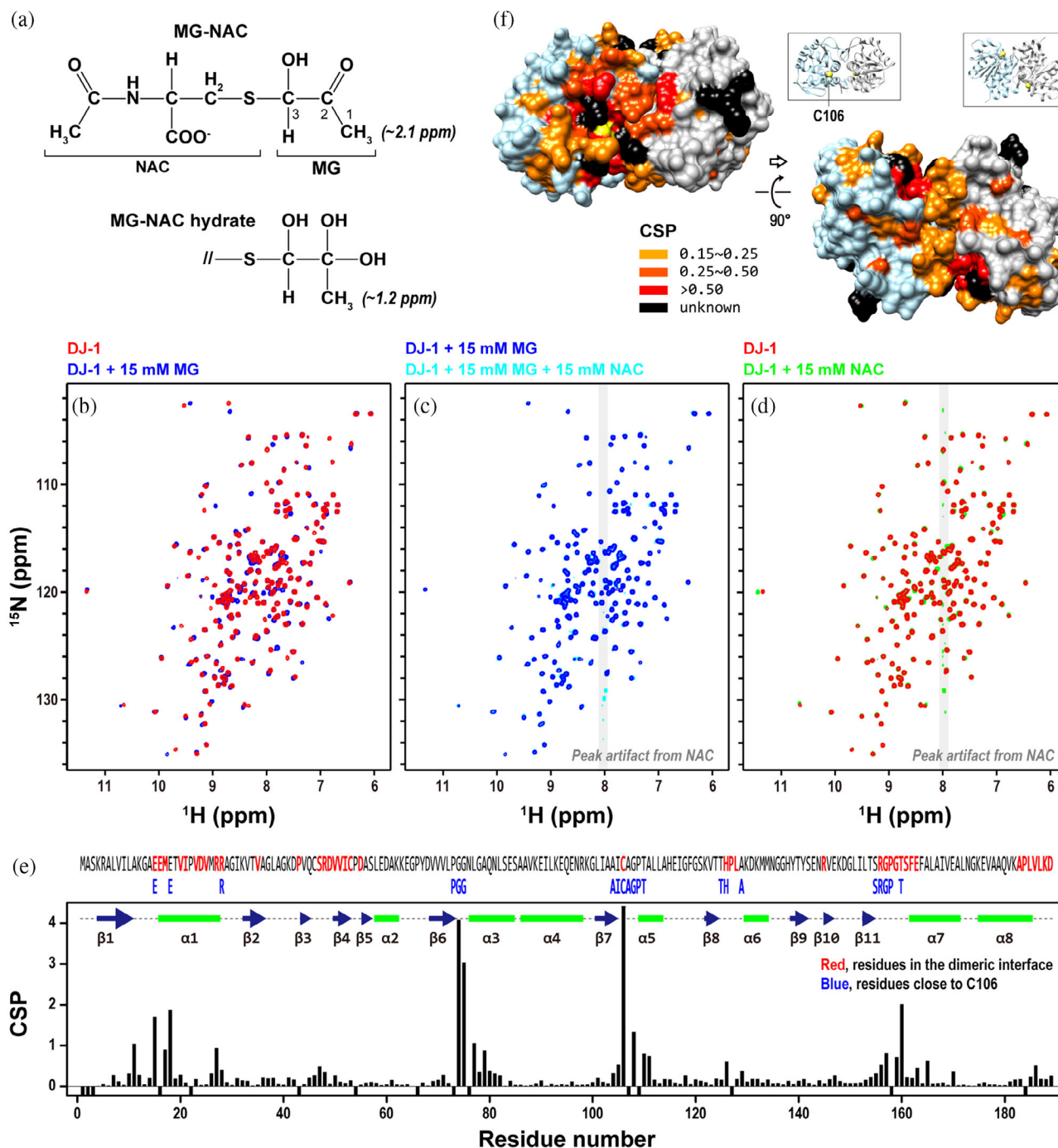
FIGURE 4 Complex state of DJ-1 and methylglyoxal (MG) in the absence and presence of 10 mM *N*-acetyl Cys (NAC). (a) The predicted chemical shift (CS) values of MG-hemiacetal of NAC (MG-NAC) likely exists as nonhydrated form, and thus the sulfur atom of C106 is only accessible to the C3 of MG and the C2 of MG-NAC. The predicted CSs of the MG-methyl protons in both hydrated and nonhydrated forms of MG-NAC are shown. (b) The ^{1}H-^{15}N heteronuclear single quantum coherence (HSQC) spectra of ^{15}NDJ-1 in the presence (MG-C106 hemiacetal) and absence of 15 mM MG are overlaid. (c) The HSQC spectra of ^{15}NDJ-1 in the presence of 15 mM MG or MG-NAC are overlaid. (d) The ^{1}H-^{15}N HSQC spectra of ^{15}NDJ-1 in the presence and absence of 15 mM NAC are overlaid. (e) The chemical shift perturbations (CSPs) of ^{15}NDJ-1 induced by the MG covalent complex are shown as a bar plot. The residues for which the HSQC crosspeaks were not shown in the free form are shown as negative bars. (f) The residues showing a strong, medium and weak CSPs are decorated in the surface models of the DJ-1 dimer structure that was generated using the crystal symmetry of the previously reported PDB structure (1SOA). Each ribbon model with the same orientation is also shown as an orientational reference (boxed).

the presence of (i) 10 mM MG and (ii) 10 mM MG and NAC (∼80% MG-NAC), to obtain the HSQC spectra of the hemithioacetal ^{15}N DJ-1 complexes (MG-C106 hemithioacetals). The HSQC spectrum of ^{15}N DJ-1 in the presence of MG was initially different from that of free ^{15}N DJ-1 (Figure 4b) and finally returned to that of free ^{15}N DJ-1 (not shown). The HSQC spectra of ^{15}N DJ-1 for the two different substrates (MG vs. MG-NAC) were almost identical (Figure 4C). The HSQC spectrum, in the presence of 10 mM NAC, showed that the interaction between NAC and ^{15}N DJ-1 was very small (Figure 4d). Interestingly, the covalent attachment of MG to C106 resulted in chemical shift perturbations (CSPs) not only in the active site pocket but also in the dimeric interfaces of DJ-1, including the middle of α1, β3–β4, and C-terminal region (Figure 4e,f). Moreover, the CSPs of ^{15}N DJ-1 induced by the attachment of MG are similar to those previously reported for C106 oxidation (sulfinic vs. thiol; Barbieri & Luchinat, 2019).

We also estimated the activation energies of DJ-1-mediated catalysis (k_{cat}) for MG and MG-GSH by varying the temperature of the ITC experiments from 20°C to 35°C. The activation energies were identical for the two substrates (Figure 5), reflecting an identical transition state. Therefore, DJ-1 is glyoxalase III, not a deglycase, in terms of the MG-C106 complex structure and activation energy. Another possibility that DJ-1 only has lower K_m value for MG-NAC and MG-GMP than for MG alone was also invalid, since the presence of NAC or GMP slowed down the lactate production by DJ-1 catalysis (Figure 2b).
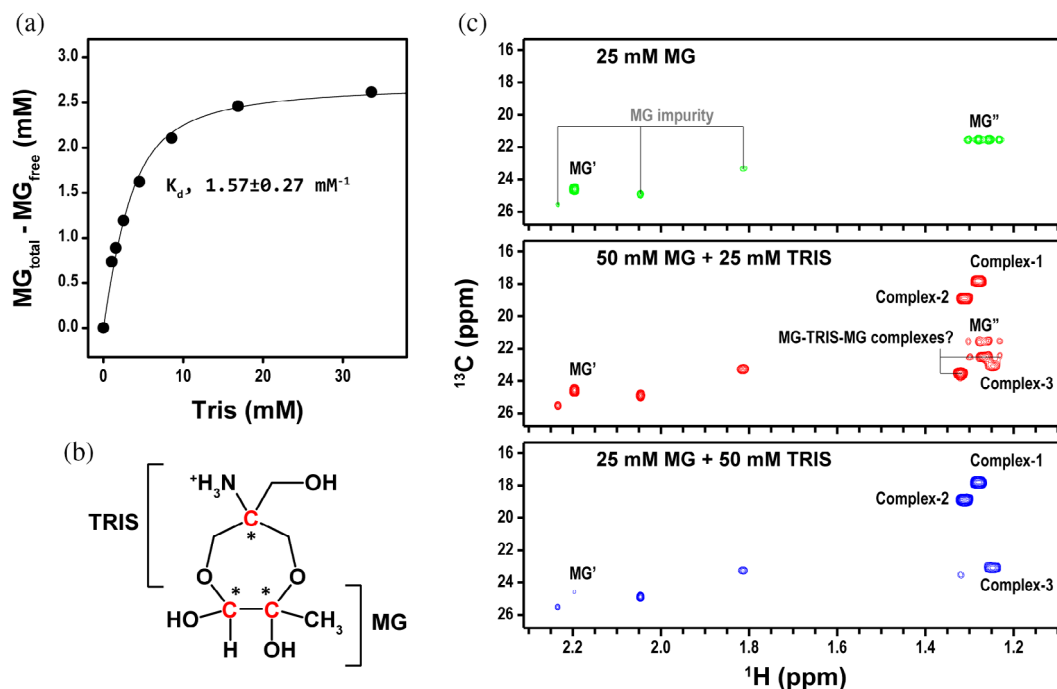
2.6 | MG forms the diastereomeric complexes with TRIS molecule in solution

Although the in vitro Cys deglycase activity of DJ-1 has been reported as an artifact of TRIS buffer (Pfaff et al., 2017), the detailed mechanism of the TRIS effect has not been determined. Since the amine of TRIS exists in a charged form (NH3$^+$) at neutral pH, we hypothesized that the three OH groups of TRIS molecules could be involved in a covalent complex with MG. The formation of the MG-TRIS complexes was investigated using NMR. Indeed, TRIS was able to form stable complexes with MG, and the K_d value (1.57 mM) was determined by tracing the methyl peaks of MG′ and MG″ with increasing TRIS concentrations (Figure 6a and Table 1). Although eight diastereomeric configurations are possible for three de novo stereospecific carbon atoms of the MG-TRIS complex, the natural abundance ^{1}H-^{13}C HSQC spectra showed that the MG-TRIS complexes mainly existed as three major diastereomers (Figure 6c). Most of all peaks resulting from the MG-TRIS complexes (Adeva-Andany et al., 2014; Allaman et al., 2015; Andreeva et al., 2019) were assigned using 2D ^{1}H-^{13}C HSQC and heteronuclear multiple bond correlation (HMBC), in addition to 1D ^{1}H NMR and distortionless enhancement by polarization transfer (DEPT) NMR experiments (Figure S6 and Table S1). The measured K_d value likely supports the hypothesis that the presence of TRIS buffer in the protein stock solution mimics the effect of MG catalysis during the activity assay of deglycase.

2.7 | Estimation of the DJ-1 glyoxalase III activity in the depletion of oxygen

DJ-1 has fewer conserved active-site residues than Hsp31, and its k_{cat} value for PG is 54 times smaller than that of Hsp31. However, the K_m value of DJ-1 is unexpectedly 22 times smaller than that of Hsp31 (Choi et al., 2014). Since the C106 residue is readily oxidized, the dissolved O$_2$ may induce the labile intermediate state of C106-sulfenic acid, which could be a reason for the decreased K_m of DJ-1. It has been reported that sulfenic acid can react as both nucleophile and electrophile according to two different tautomers (sulfenyl and sulfinyl; Freeman, 2015; Kumar & Farmer, 2017). Since the sulfenyl form of the C106-sulfenic acid might have a higher affinity for MG, we measured the K_m and k_{cat}

FIGURE 5 Arrhenius plots of the DJ-1-mediated catalysis for methylglyoxal (MG) and MG-hemiacetal of glutathione (MG-GSH). The single-shot isothermal titration calorimetry experiments using 20 μM DJ-1 were done in the presence of MG alone (3 mM) or MG-GSH (3 mM MG and 10 mM GSH). The temperature-dependent V_{max} values were calculated for the cases of MG alone and MG-GSH, respectively. The activation energies of the DJ-1-mediated MG catalysis are almost identical for both cases of MG alone and MG-GSH.

FIGURE 6 Characterization of the methylglyoxal (MG)-TRIS diastereomeric complex. The binding event between MG and TRIS molecules is under the NMR time scale of slow exchange, and the concentration of free MG was determined by integrating the methyl peaks of MG′ and MG″. (a) The K_d value between MG and TRIS molecule was determined from the TRIS-bound fraction of MG as increasing the concentrations of TRIS. The MG-TRIS complex formation results in three de novo stereospecific carbon atoms (indicated with stars). (b) The chemical structure of the MG-TRIS complex, in which three de novo diastereotopic carbon atoms are red-colored and indicated by stars. (c) The natural abundance ^{1}H-^{13}C heteronuclear single quantum coherence (HSQC) spectra of MG alone (top), MG-TRIS (2:1) (middle), and MG-TRIS (1:2) (bottom). The major MG-TRIS diastereomers (complex-1, complex-2, and complex-3) are indicated in the natural abundance ^{1}H-^{13}C HSQC spectra. The peak integral of the complex-3 was half that of the complex-1 and complex-2. Although additional sets of very tiny peaks (<5% peak intensity compared with that of the major sets) were still not assigned likely due to the presence of impurities or unidentified additional MG-TRIS covalent complexes, the major three sets of peaks are clearly assigned as different diastereotopic isomers of the MG-TRIS complexes.

values of DJ-1 for PG under O_2-depleted conditions using N_2-purge. However, the measured values (K_m, 11.8 ± 2.4 vs. 12.1 ± 2.2 μM; k_{cat}, 0.0228 ± 0.0014 vs. 0.0234 ± 0.0013 s^{-1}) were almost identical for both cases in the absence and presence of N_2-purging (Figure S7), suggesting that the glyoxalase III activity of DJ-1 is not dependent on the C106-sulfenic acid form.

3 | DISCUSSION

3.1 | In vivo glyoxalase III activity of DJ-1

The estimated concentration of MG in tissues (1–5 μM) is much lower than that in plasma (0.1–400 μM) (Allaman et al., 2015; Maessen et al., 2015). The consideration of both attached and free MG molecules increases the effective concentration up to 310 μM in cultured CHO cells (Chaplen et al., 1998). Therefore, glyoxalase activity is

likely essential for homeostasis in highly metabolic living organisms. It has recently been reported that DJ-1 prevents damages to proteins and metabolites caused by the reactive glycolytic metabolite (1,3-bisphosphoglycerate; Heremans et al., 2022). Although the catalytic activity of DJ-1 is very low compared to that of glyoxalase I/II system using GSH (Thornalley, 1990), it has been reported that enzymes operating during secondary metabolism are ∼ 30 times less active on average than those during central metabolism (Bar-Even et al., 2011). DJ-1 could be effective as a secondary activity (glyoxalase III) when the primary glyoxalase I/II system is impaired, likely because of oxidative stress, which decreases the in vivo concentration of GSH.

Although the highly efficient glyoxalase I/II system catalyzes MG only to D-lactate, the lactate enantiomers of different glyoxalase III enzymes vary. Hsp31 and atDJ-1d produce a mixture of D/L-lactate and only D-lactate, respectively, but the specific active-site configuration of DJ-1 only results in L-lactate production by

compensating for absolute enzyme activity (Choi et al., 2014). DJ-1 activity would be beneficial because L-lactate is utilized as a major energy source in the brain, and its oxidative conversion to pyruvate by L-LDH is also accompanied by the production of NADH from NAD^+ (Adeva-Andany et al., 2014).

3.2 | Correlation between the structural perturbation and various in vivo interactions of DJ-1

There have been many reports showing that DJ-1 regulates various in vivo functions through the interaction with other proteins including α-synuclein (Zondler et al., 2014), p53 (Fan et al., 2008), PTEN, Ask1, BcL-X_L, and so forth (Dolgacheva et al., 2019). Interestingly, these relatively strong in vivo interactions have yet to be reproduced by the in vitro experiments clearly. Recent in vitro CSP NMR experiments have shown that (i) H_2O_2-treated DJ-1 only displays a weak interaction with ^{15}N-labeled BcL-X_L but (ii) the C-terminal α-helical peptide of DJ-1 alone appreciably binds to the hydrophobic pocket of BcL-X_L, which is not possible in the native DJ-1 structure (Lee et al., 2018). The k_{cat} value of DJ-1 for MG (0.263 s^{-1} at 35°C) seems to be very low, and it would be possible to provide a different point of view based on (i) the very low k_{cat} value of DJ-1 and (ii) its interaction with BcL-X_L. We speculated that DJ-1 could initiate a certain process via a protein–protein interaction that is dependent on a structural change induced by MG-C106 hemiacetal or C106 sulfinic acid. The structural perturbation of DJ-1 by the MG attachment or C106-oxidation in the regions of the dimeric interface including the C-terminal helix might be related to the unreproduced in vivo interactions of DJ-1 protein.

4 | CONCLUSIONS

DJ-1 is involved in the etiology of many aging-related diseases including PD, and thus resolving the exact activity (glyoxalase III vs. deglycase) is critical for interpreting the actual in vivo functions and disease onset mechanism of DJ-1. The previously reported deglycase activity of DJ-1, which only works for the early glycated species, clearly resorts to the reversibility of the early glycated products to free MG and unmodified substrates (Andreeva et al., 2019). Here, the kinetic studies of DJ-1-mediated MG catalysis using ITC and NMR clarified that DJ-1 has only glyoxalase III activity by resolving detailed time-dependent changes of each reaction component and by characterizing a catalysis intermediate. The stable diastereomeric complexes of MG with TRIS can also be explained by the presence of its three

OH groups, since MG exists in hydrated forms (MG′ and MG″) in aqueous solutions.

5 | MATERIALS AND METHODS

5.1 | Preparation of DJ-1 proteins and chemical stock solutions

Pure native DJ-1 protein was prepared following a recently reported column chromatography method (Choi et al., 2022). The purified DJ-1 protein (∼0.5 mM) in non-buffered 50 mM NaCl solution was stored at −70°C before use, and the concentration was determined by UV absorption at 280 nm using the extinction coefficient (4470 M^{-1}·cm^{-1}; Pace et al., 1995). The N_2-purging during chromatography purifications prevented the oxidation of DJ-1, even in the absence of dithiothreitol. All experiments, including NMR acquisitions, were conducted in a buffer (pH 7.0, 50 mM Na-phosphate, and 50 mM NaCl), unless specifically mentioned.

All the materials including MG, NAC, GSH, GMP, D/L-lactates, and D/L-LDH (D-LDH/L-LDH) were purchased from Sigma-Aldrich. Since the concentrations of NAC, GSH, and GMP were relatively high (up to 10 mM), the pH of the 0.2 M NAC, GSH, and GMP stock solutions was first adjusted to near 7.0, to maintain the pH of the experimental buffers. To measure the concentration of MG stock solution (40%, Sigma-Aldrich), the UV absorption at 288 nm was measured using a Nanodrop 2000 (Thermo Scientific) by increasing the concentration of MG at a fixed concentration of NAC (100 mM). The UV absorption increased with an increase in the ratio of MG to NAC, and the increasing slope changed after the point of the equivalent molar ratio. The exact concentration of the 40% MG stock solution (3.5 M) was back-calculated based on 100 mM NAC.

5.2 | K_d measurements of the MG-intermediates

The K_d values of the MG-hemiacetals (MG-GSH and MG-NAC) were estimated using UV absorption (288 nm) at room temperature with varying concentrations of titrants and fixed concentrations of MG (3 mM). To estimate the K_d value of the MG-NAC and the MG hemiaminal of GMP (MG-GMP), the 1D NMR spectra of 3 mM MG with different concentrations of NAC or GMP were measured using a 700 MHz NMR spectrometer equipped with a TCI-cryoprobe (Bruker) at 25°C after preincubation for 1.0 h. The K_d of the MG-TRIS complex was also estimated using 1D NMR spectroscopy, in which the pH of the TRIS buffer was adjusted to

7.0. The concentration of MG-GSH ([MG]$_{bound}$) is expressed as a function of the K_d value and the total concentrations of MG and GSH ([MG]$_{total}$ and [GSH]$_{total}$); [MG]$_{bound}$ = (Q1/2 × [MG]$_{total}$) × {([GSH]$_{total}$ + [MG]$_{total}$ + K_d) − SQRT [([GSH]$_{total}$ + [MG]$_{total}$ + K_d)^2 − (4 × [GSH]$_{total}$ × K_d)]}. The factor of Q1 is an additional fitting parameter to normalize the measured values.

5.3 | ITC monitoring the MG-catalysis

Single-shot ITC experiments were performed using a MicroCal Auto-iTC200 instrument (Malvern Instruments) at 35°C. The concentration of DJ-1 and the reaction temperature were increased to reduce the experiment time to within the allowed acquisition time of a single shot. DJ-1 protein was completely stable at 35°C, since no spectral changes were identified in the HSQC spectrum of 0.2 mM ^{15}NDJ-1 at least for 1 day, and only a small amount of precipitated ^{13}C/^{15}N-labeled DJ-1 (^{13}C/^{15}NDJ-1) was identified after several days of NMR experiments at 35°C (not shown). The concentrated DJ-1 protein in the syringe was injected into a mixing cell (20-fold dilution) containing 1 mM MG alone or 1 mM MG-mixtures of NAC or GMP (1, 2, 4, and 8 mM). The heat changes induced by the injection of the same volume of buffer were <5% of those of DJ-1-mediated MG catalysis, and the effect of the blank injection was no longer considered. The kinetic parameters (K_m and k_{cat}) were determined by two different methods for the single-shot ITC profiles: (i) The Michaelis–Menten equation was used under the assumption that the reaction rate and the total amount of MG are proportional to the rate of heat change and the total amount of heat production, respectively (Quinn & Hansen, 2019). (ii) The kinetic parameters were derived by the direct fitting of the whole ITC profiles using the Lambert W(x) function (Golicnik, 2010) as the previously reported method (Transtrum et al., 2015).

5.4 | ^{1}H-^{15}N HSQC experiments of ^{15}NDJ-1 in the presence of MG and MG-NAC

All HSQC spectra were recorded in 800 or 900 MHz NMR spectroscopy equipped with a TCI-cryoprobe

(Bruker) at 25°C. The samples were prepared in buffer (pH 7.0, 75 mM HEPES, 50 mM NaCl, and 5% D$_2$O), in which HEPES instead of phosphate was used for a better signal-to-noise ratio of the cryoprobe at higher buffer concentrations. The HSQC spectra of 0.2 mM ^{15}NDJ-1 in the absence and presence of 10 mM NAC were recorded as references. The time-course HSQC spectra of 0.2 mM ^{15}NDJ-1 in the presence of 10 mM MG or MG-NAC were recorded until the spectra returned to that of free ^{15}NDJ-1. The CSP values were calculated from the equation, square root of [(6 × ΔH)^2 + ΔN^2], as the average distribution of the amide ^{15}N chemical shifts (CSs) was 6-fold greater than that of ^{1}H CSs (Lee et al., 2022).

5.5 | Kinetic analyses of MG catalysis by 1D NMR

DJ-1 (15 μM) was incubated with 5 mM MG, MG-NAC, and MG-GMP in NMR tubes, and real-time changes in the reaction components were traced using 1D NMR spectra at 25°C. The original 1D NMR pulse sequence (zgesgppe) was modified as a pseudo-2D version for time-resolved experiments, and each 1D spectrum was recorded at 3 min intervals with 5 s of experimental time delay (d1). The time-resolved pseudo-2D data were processed using the NMRPipe program (Delaglio et al., 1995), and the kinetic parameters were determined using the parameter fitting method of ordinary differential equations with the MATLAB software. MG exists as monohydrated (MG′) and dihydrated (MG″) forms in solution, the terms containing the nonhydrated form (MG) could be ignored (Equation 1). Since the enzyme kinetic parameters of DJ-1 (K_m and k_{cat}) were measured for the overall MG amount ([MG]$_{sum}$), not for a specific MG′ or MG″, the fraction factors (Equation 2) were applied to the differential equations of MG′ and MG″ (Equations 3 and 4). The time-dependent concentrations of all components were fitted to the following differential equations (Equations 3–6).

$$[MG]_{sum} = [MG] + [MG'] + [MG''] \cong [MG'] + [MG''] \quad (1)$$

$$f_{[MG']} = 1 - f_{[MG'']} = [MG']/[MG]_{tot} \cong [MG']/([MG'] + [MG'']) \quad (2)$$

$$d[MG']/dt \cong k_3[MG''] - (k_{-3} + k_2)[MG'] - \frac{d[LAC]}{dt} \cdot f_{[MG']} + \left(k_{-4}[MG:GMP] - k_4^{app}[GMP]([MG'] + [MG'']) \right) \cdot f_{[MG']} \quad (3)$$

$$d[\text{MG}'']/dt \cong k_{-3}[\text{MG}'] - k_3[\text{MG}''] - d[\text{LAC}]/dt \cdot f_{[\text{MG}'']} + \left(k_{-4}[\text{MG}:\text{GMP}] - k_4^{\text{app}}[\text{GMP}]([\text{MG}'] + [\text{MG}''])\right) \cdot f_{[\text{MG}'']} \quad (4)$$

$$d[\text{GMP}]/dt = -d[\text{MG}:\text{GMP}]/dt$$
$$\cong k_{-4}[\text{MG}:\text{GMP}] - k_4^{\text{app}}[\text{GMP}]([\text{MG}'] + [\text{MG}'']) \quad (5)$$

$$d[\text{LAC}]/dt \cong k_{\text{cat}} \cdot [\text{DJ1}]_0$$
$$\cdot ([\text{MG}'] + [\text{MG}''])/(K_M + ([\text{MG}'] + [\text{MG}''])) \quad (6)$$

The k_3 of the exchange between MG′ and MG″ was estimated from the equation, $\Delta M_z^{\text{MG}'} = k_3 T_1^{\text{sat}} M_z^{\text{MG}'}$, in which $\Delta M_z^{\text{MG}'}$ is the difference of the steady-state magnetizations of MG′—CH$_3$ in the presence and absence of the saturation of the MG″—CH$_3$ peak, and T_1^{sat} $[=T_1^{\text{MG}'}/(1 + k_3 T_1^{\text{MG}'})]$ is the T_1 value of the MG′—CH$_3$ peak estimated during the saturation of the MG″—CH$_3$ peak (Robinson et al., 1984). Because [MG] (two ketone forms) in solution is extremely small, the k_3/k_{-3} value was almost the same as the [MG′]/[MG″] value.

5.6 | Characterization of D/L-lactate products

To measure the relative amounts of D-lactate and L-lactate enantiomers in the DJ-1 catalyzed reactions of MG, MG-NAC, and MG-GMP, the relative activity of D-LDH and L-LDH was first estimated individually for each 0.2 mM D-lactate and L-lactate, respectively, in the LDH-reaction buffer (pH 9.5, 50 mM glycine, 50 mM NaCl, 50 mM hydrazine, and 2 mM NAD$^+$). Interestingly, the activity of D-LDH was ∼12 times lower than that of L-LDH. Therefore, the amount of D-LDH used was 12 times higher than that of L-LDH during the enzymatic reactions. First, 1 mM MG was mixed with the different concentrations of NAC or GMP, and then lactate production was completed with 20 μM DJ-1 overnight. Each reactant was diluted 5-fold with LDH-reaction buffer, and the reactions with L-LDH and D-LDH were monitored at 340 nm using a UV-visible microplate reader (VersaMax).

5.7 | Characterization of the TRIS-MG diastereomers by NMR

A mixture of 25 mM MG and 50 mM TRIS allowed most MG molecules to form a complex with TRIS in buffer (pH 7.0, 50 mM Na-phosphate, and 50 mM NaCl). The pH of the TRIS stock solution (0.2 M) was adjusted to 7.0 before mixing with MG. We recorded the ^{1}H-^{13}C HSQC and HMBC, ^{1}H-^{1}H correlated spectroscopy (COSY), and rotating frame Overhauser effect spectroscopy (ROESY), and 1D ^{13}C DEPT using 700 MHz NMR equipped with a TCI-cryoprobe at 25°C. All spectra were processed using the NMRPipe program (Delaglio et al., 1995) and the assignment of CSs was performed using the POKY software (Lee et al., 2021).

5.8 | Enzyme assay of DJ-1 using PG under oxygen-depleted condition

The PG catalysis mediated by DJ-1 was assessed following a previously reported method (Choi et al., 2014), except for N$_2$-purging to deplete the dissolved oxygen. The enzymatic reaction was executed with 2.5 μM DJ-1 in buffer (pH 7.5, 50 mM HEPES, 100 mM NaCl) by varying the concentrations of PG (5, 10, 20, 30, 50, and 80 μM) at 35 °C. The reaction buffer was purged with N$_2$ gas for 30 min, and then the subsequent dispenses of the buffer and PG stock solution to six UV cuvettes were performed in the N$_2$ chamber, in which the oxygen concentration was 0.6%. The cuvettes were quickly moved to the UV–visible spectrophotometer (Varian Cary 400 Bio), and then a small volume of the DJ-1 stock solution (0.15 mM) was added to each cuvette. The time-course UV absorption of all six cuvettes at 250 nm was measured by applying N$_2$-purging on the spectrophotometer. The same control experiments were done without N$_2$-purging.

ORCID

Joonhyeok Choi https://orcid.org/0000-0002-3800-0394
Kyoung-Seok Ryu https://orcid.org/0000-0002-8422-6669

REFERENCES

Adeva-Andany M, Lopez-Ojen M, Funcasta-Calderon R, Ameneiros-Rodriguez E, Donapetry-Garcia C, Vila-Altesor M, et al. Comprehensive review on lactate metabolism in human health. Mitochondrion. 2014;17:76–100.

Allaman I, Belanger M, Magistretti PJ. Methylglyoxal, the dark side of glycolysis. Front Neurosci. 2015;9:23.

Andreeva A, Bekkhozhin Z, Omertassova N, Baizhumanov T, Yeltay G, Akhmetali M, et al. The apparent deglycase activity of DJ-1 results from the conversion of free methylglyoxal present in fast equilibrium with hemithioacetals and hemiaminals. J Biol Chem. 2019;294:18863–72.

Ariga H, Takahashi-Niki K, Kato I, Maita H, Niki T, Iguchi-Ariga SM. Neuroprotective function of DJ-1 in Parkinson's disease. Oxidative Medicine and Cellular Longevity. 2013;2013:683920.

Barbieri L, Luchinat E. Backbone resonance assignment of human DJ-1 in the reduced state and in the cysteine sulfinic acid state. Biomol NMR Assign. 2019;13:371–6.

Bar-Even A, Noor E, Savir Y, Liebermeister W, Davidi D, Tawfik DS, et al. The moderately efficient enzyme: evolutionary and physicochemical trends shaping enzyme parameters. Biochemistry. 2011;50:4402–10.

Bonifati V, Rizzu P, van Baren MJ, Schaap O, Breedveld GJ, Krieger E, et al. Mutations in the DJ-1 gene associated with autosomal recessive early-onset parkinsonism. Science. 2003; 299:256–9.

Canet-Aviles RM, Wilson MA, Miller DW, Ahmad R, McLendon C, Bandyopadhyay S, et al. The Parkinson's disease protein DJ-1 is neuroprotective due to cysteine-sulfinic acid-driven mitochondrial localization. Proc Natl Acad Sci U S A. 2004;101:9103–8.

Castillo AM, Patiny L, Wist J. Fast and accurate algorithm for the simulation of NMR spectra of large spin systems. J Magn Reson. 2011;209:123–30.

Cha SS, Jung HI, Jeon H, An YJ, Kim IK, Yun S, et al. Crystal structure of filamentous aggregates of human DJ-1 formed in an inorganic phosphate-dependent manner. J Biol Chem. 2008; 283:34069–75.

Chaplen FW, Fahl WE, Cameron DC. Evidence of high levels of methylglyoxal in cultured Chinese hamster ovary cells. Proc Natl Acad Sci U S A. 1998;95:5533–8.

Chen J, Li L, Chin LS. Parkinson disease protein DJ-1 converts from a zymogen to a protease by carboxyl-terminal cleavage. Hum Mol Genet. 2010;19:2395–408.

Choi D, Kim J, Ha S, Kwon K, Kim EH, Lee HY, et al. Stereospecific mechanism of DJ-1 glyoxalases inferred from their hemithioacetal-containing crystal structures. FEBS J. 2014;281:5447–62.

Choi J, Yoo HJ, Cho K, Kim HN, Lee JH, Ryu KS. Separation of native and C106-oxidized DJ-1 proteins by using column chromatography. Protein Expr Purif. 2022;195-196:106092.

Delaglio F, Grzesiek S, Vuister GW, Zhu G, Pfeifer J, Bax A. NMRPipe: a multidimensional spectral processing system based on UNIX pipes. J Biomol NMR. 1995;6:277–93.

Dolgacheva LP, Berezhnov AV, Fedotova EI, Zinchenko VP, Abramov AY. Role of DJ-1 in the mechanism of pathogenesis of Parkinson's disease. J Bioenerg Biomembr. 2019;51:175–88.

Fan J, Ren H, Fei E, Jia N, Ying Z, Jiang P, et al. Sumoylation is critical for DJ-1 to repress p53 transcriptional activity. FEBS Lett. 2008;582:1151–6.

Freeman F. Mechanisms of reactions of sulfur hydride hydroxide: tautomerism, condensations, and C-sulfenylation and O-sulfenylation of 2,4-pentanedione. J Phys Chem A. 2015;119: 3500–17.

Gao Q, Jacob-Dolan JW, Scheck RA. Parkinsonism-associated protein DJ-1 is an antagonist, not an eraser, for protein glycation. Biochemistry. 2023;62:1181–90.

Golicnik M. Explicit reformulations of time-dependent solution for a Michaelis-Menten enzyme reaction model. Anal Biochem. 2010;406:94–6.

Guzman JN, Sanchez-Padilla J, Wokosin D, Kondapalli J, Ilijic E, Schumacker PT, et al. Oxidant stress evoked by pacemaking in dopaminergic neurons is attenuated by DJ-1. Nature. 2010;468: 696–700.

Heremans IP, Caligiore F, Gerin I, Bury M, Lutz M, Graff J, et al. Parkinson's disease protein PARK7 prevents metabolite and protein damage caused by a glycolytic metabolite. Proc Natl Acad Sci U S A. 2022;119:e2111338119.

Jun YW, Kool ET. Small substrate or large? Debate over the mechanism of glycation adduct repair by DJ-1. Cell Chem Biol. 2020; 27:1117–23.

Kim I, Kim E, Yoo S, Shin D, Min B, Song J, et al. Ribose utilization with an excess of mutarotase causes cell death due to accumulation of methylglyoxal. J Bacteriol. 2004;186:7229–35.

Kumar MR, Farmer PJ. Trapping reactions of the Sulfenyl and sulfinyl Tautomers of sulfenic acids. ACS Chem Biol. 2017;12: 474–8.

Lee JY, Song J, Kwon K, Jang S, Kim C, Baek K, et al. Human DJ-1 and its homologs are novel glyoxalases. Hum Mol Genet. 2012; 21:3215–25.

Lee MK, Lee MS, Bae DW, Lee DH, Cha SS, Chi SW. Structural basis for the interaction between DJ-1 and Bcl-XL. Biochem Biophys Res Commun. 2018;495:1067–73.

Lee MS, Lee SO, Choi J, Ryu M, Lee MK, Kim JH, et al. MUL1-RING recruits the substrate, p53-TAD as a complex with UBE2D2-UB conjugate. FEBS J. 2022;289:3568–86.

Lee SJ, Kim SJ, Kim IK, Ko J, Jeong CS, Kim GH, et al. Crystal structures of human DJ-1 and Escherichia coli Hsp31, which share an evolutionarily conserved domain. J Biol Chem. 2003; 278:44552–9.

Lee W, Rahimi M, Lee Y, Chiu A. POKY: a software suite for multidimensional NMR and 3D structure calculation of biomolecules. Bioinformatics. 2021;37(18):3041–2.

Lo TW, Westwood ME, McLellan AC, Selwood T, Thornalley PJ. Binding and modification of proteins by methylglyoxal under physiological conditions. A kinetic and mechanistic study with N alpha-acetylarginine, N alpha-acetylcysteine, and N alpha-acetyllysine, and bovine serum albumin. J Biol Chem. 1994; 269:32299–305.

Maessen DE, Stehouwer CD, Schalkwijk CG. The role of methylglyoxal and the glyoxalase system in diabetes and other age-related diseases. Clin Sci (Lond). 2015;128:839–61.

Mazza MC, Shuck SC, Lin J, Moxley MA, Termini J, Cookson MR, et al. DJ-1 is not a deglycase and makes a modest contribution to cellular defense against methylglyoxal damage in neurons. J Neurochem. 2022;162:245–61.

Nagakubo D, Taira T, Kitaura H, Ikeda M, Tamai K, Iguchi-Ariga SM, et al. DJ-1, a novel oncogene which transforms

mouse NIH3T3 cells in cooperation with ras. Biochem Biophys Res Commun. 1997;231:509–13.

Pace CN, Vajdos F, Fee L, Grimsley G, Gray T. How to measure and predict the molar absorption coefficient of a protein. Protein Sci. 1995;4:2411–23.

Pfaff DH, Fleming T, Nawroth P, Teleman AA. Evidence against a role for the parkinsonism-associated protein DJ-1 in methylglyoxal detoxification. J Biol Chem. 2017;292:685–90.

Quinn CF, Hansen LD. Enzyme kinetics determined by single-injection isothermal titration calorimetry. Methods Mol Biol. 2019;1964:241–9.

Rae C, Berners-Price SJ, Bulliman BT, Kuchel PW. Kinetic analysis of the human erythrocyte glyoxalase system using 1H NMR and a computer model. Eur J Biochem. 1990;193:83–90.

Richarme G. Response to manuscript by Pfaff et al.: evidence against a role of DJ-1 in methylglyoxal detoxification. J Biol Chem. 2017;292:12783.

Richarme G, Liu C, Mihoub M, Abdallah J, Leger T, Joly N, et al. Guanine glycation repair by DJ-1/Park7 and its bacterial homologs. Science. 2017;357:208–11.

Richarme G, Mihoub M, Dairou J, Bui LC, Leger T, Lamouri A. Parkinsonism-associated protein DJ-1/Park7 is a major protein deglycase that repairs methylglyoxal- and glyoxal-glycated cysteine, arginine, and lysine residues. J Biol Chem. 2015;290:1885–97.

Robinson G, Chapman BE, Kuchel PW. 31P NMR spin-transfer in the phosphoglyceromutase reaction. Eur J Biochem. 1984;143:643–9.

Ryu KS, Kim C, Kim I, Yoo S, Choi BS, Park C. NMR application probes a novel and ubiquitous family of enzymes that alter monosaccharide configuration. J Biol Chem. 2004;279:25544–8.

Subedi KP, Choi D, Kim I, Min B, Park C. Hsp31 of *Escherichia coli* K-12 is glyoxalase III. Mol Microbiol. 2011;81:926–36.

Thornalley PJ. The glyoxalase system: new developments towards functional characterization of a metabolic pathway fundamental to biological life. Biochem J. 1990;269(1):1–11.

Transtrum MK, Hansen LD, Quinn C. Enzyme kinetics determined by single-injection isothermal titration calorimetry. Methods. 2015;76:194–200.

van der Brug MP, Blackinton J, Chandran J, Hao LY, Lal A, Mazan-Mamczarz K, et al. RNA binding activity of the recessive parkinsonism protein DJ-1 supports involvement in multiple cellular pathways. Proc Natl Acad Sci U S A. 2008;105:10244–9.

Witt AC, Lakshminarasimhan M, Remington BC, Hasim S, Pozharski E, Wilson MA. Cysteine pKa depression by a protonated glutamic acid in human DJ-1. Biochemistry. 2008;47:7430–40.

Zondler L, Miller-Fleming L, Repici M, Goncalves S, Tenreiro S, Rosado-Ramos R, et al. DJ-1 interactions with alpha-synuclein attenuate aggregation and cellular toxicity in models of Parkinson's disease. Cell Death Dis. 2014;5:e1350.

SUPPORTING INFORMATION

Additional supporting information can be found online in the Supporting Information section at the end of this article.